Journal of Volcanology and Geothermal Research 472 (2026) 108564

Contents lists available at ScienceDirect

Journal of Volcanology and Geothermal Research

journal homepage: www.journals.elsevier.com/journal-of-volcanology-and-geothermal-research

New precisely dated pyroclastic deposits from Pliocene-Pleistocene volcanic activity in the central parts of Southeastern Europe

Kata Molnár [a,*], Pierre Lahitte [b], Zsolt Benkó [a,c], János Szepesi [a,d], Maxim Portnyagin [e], Daniel Frick [f], Samuele Agostini [g], Sebastien Nomade [h], Maria Giuditta Fellin [i], Colin Maden [i], Ivan Boev [j], Blažo Boev [j], Marjan Temovski [a,c]

[a] HUN-REN Institute for Nuclear Research (ATOMKI), Debrecen, Hungary
[b] Laboratoire GEOPS, Université Paris-Saclay, CNRS, France
[c] Department of Mineralogy and Geology, University of Debrecen, Hungary
[d] MTA–HUN-REN CSFK Lendület "Momentum" PannonianVolcano Research Group, Institute for Geological and Geochemical Research, HUN-REN Research Centre for Astronomy and Earth Sciences, Budapest, Hungary
[e] GEOMAR Helmholtz Centre for Ocean Research, Kiel, Germany
[f] Institute for Geosciences, Christian-Albrecht University, Kiel, Germany
[g] Istituto di Geoscienze e Georisorse, Consiglio Nazionale delle Ricerche, Pisa, Italy
[h] Laboratoire des Sciences du Climat et de l'Environnement, CEA, LSCE/IPSL, Université Versailles Saint Quentin et Paris-Saclay, France
[i] ETH Zurich, Department of Earth and Planetary Sciences, Zurich, Switzerland
[j] Goce Delčev University, Štip, Macedonia

ARTICLE INFO

Keywords:
Pyroclastics
Tephrochronology
Mediterranean
Sanidine Ar/Ar dating
Explosive-effusive transition

ABSTRACT

Single-crystal sanidine $^{40}Ar/^{39}Ar$ dating revealed at least six new explosive eruption events during the 4.0–3.5 Ma and 3.0–2.5 Ma periods in the eruptive history of the Kožuf-Voras volcanic system located in the central parts of Southeastern Europe. The precise ages helped to redefine the timing and eruptive style of the volcanic system, as the 4.0–2.5 Ma period was previously considered as mainly quiescent, with dominantly lava dome building activity recognized so far. The pyroclastic layers (mainly massive tuff-lapilli tuff and massive lithic breccia) are deposited from phreatomagmatic and subplinian eruptions, and block-and-ash flows in the volcano-sedimentary Mariovo basin, west of the volcanic system. The newly recognized pyroclastic layers could serve as regional marker layers, as neither their ages nor their geochemical and isotopic (bulk and glass) compositions overlap with those previously studied tephra layers, either from the Kožuf-Voras volcanic system or from other volcanic sources (e.g., Aegean arc). Differences in the geochemical and isotopic data imply sequential evacuation of closely emplaced, discrete, melt-dominant bodies during the older period. In contrast, the younger sequence might represent a compositionally zoned single melt body. The latter also represents an explosive-to-effusive transition as the top layer is a block-and-ash flow unit resulting from a dome collapse.

1. Introduction

Widespread magmatism characterized the circum-Mediterranean region during Cenozoic times producing primarily effusive volcanic products with minor pyroclastic deposits (e.g., Harangi et al., 2006; Lustrino and Wilson, 2007). During the Pliocene-Quaternary period, volcanic activity was mainly focused on the central (e.g., Peccerillo, 2005) and eastern parts of the Mediterranean region (e.g., Agostini et al., 2007; Pe-Piper and Piper, 2007) with few volcanoes remaining active until the present day (e.g., Etna). Although the volcanism was mainly effusive, the preservation of pyroclastic deposits related to subordinate explosive activity has broader significance for the circum-Mediterranean region.

Tephra occurrences are of key importance to date and link paleoenvironmental or geological events (e.g., Lane et al., 2017; Lowe, 2011; Tomlinson et al., 2015). Tephrochronology can help to correlate far-reaching (and preserved) tephra horizons (e.g., Brlek et al., 2024), to understand the dynamics of highly explosive volcanic systems, to give an insight into pre-eruptive magmatic processes, and to provide independent markers for environmental and climate changes in both marine

* Corresponding author.
E-mail address: molnar.kata@atomki.hu (K. Molnár).

https://doi.org/10.1016/j.jvolgeores.2026.108564
Received 10 February 2026; Accepted 10 February 2026
Available online 14 February 2026

and terrestrial sedimentary successions (e.g., coal layers, lake sediments, deep-sea sediments or ice; Clift and Blusztajn, 1999; Hutchison et al., 2024; Keller et al., 1978; Steenbrink et al., 1999; Wagner et al., 2019).

The central parts of Southeastern Europe (i.e., the Balkan Peninsula; Fig. 1) were also characterized by extensive volcanism, related to the tectonic evolution of the Alpine-Mediterranean region (Schmid et al., 2020 and references therein). Two main periods of magmatic activity are known: Early Oligocene (ca. 33–29 Ma; Boev and Yanev, 2001; Lehmann et al., 2013) and Late Miocene-Pleistocene (ca. 8–1.5 Ma; Cvetković et al., 2004; Janković et al., 1997; Kolios et al., 1980; Molnár et al., 2022; Yanev et al., 2008). In the younger period, scattered ultrapotassic mafic centers developed exclusively in the Vardar zone (Arsovski, 1997), typically along the margins of extensional basins (Dumurdzanov et al., 2005; Molnár et al., 2022; Yanev et al., 2008), which development is linked to the propagation of the North Anatolian fault and the retreating Hellenic slab (Burchfiel et al., 2008; Dumurdzanov et al., 2005). Contemporaneously, the high-K calc-alkaline – shoshonitic Kožuf-Voras volcanic system (hereafter KV; Fig. 1) also developed in the Vardar zone, possibly related to the ongoing subduction along the Hellenic slab, representing the northernmost volcanic system (Molnár et al., 2022, 2023; Yanev et al., 2008).

Here, we present for the first time evidences of Pliocene-Pleistocene pyroclastic occurrences related to the KV. This activity is now precisely constrained by new radioisotopic ages and characterized geochemically on whole-rock (major, trace elements and Sr—Nd isotopes) as well as glass geochemistry (major and trace elements). These newly discovered explosive phases are potentially new regional markers and decipher the evolution of KV, with possible significance for understanding the evolution of the surrounding basins.

2. Geological background

The KV developed between 6.5 and 1.8 Ma, extending in a SW-NE direction along the Macedonian-Greek border. The volcanic system is located in the western part of the Vardar zone and formed dominantly on its pre-Cenozoic basement (i.e., the Late Cretaceous cover of the Pelagonian massif, the Jadar-Kopaonik unit, the Sava suture zone and the Circum-Rhodope unit; Schmid et al., 2020). The volcanism of KV is characterized mainly by lava dome-forming activity with minor explosive eruptions (Boev and Ivanova, 2024; Janković et al., 1997; Kolios et al., 1980; Molnár et al., 2022, 2023). The ages of the eruption centers decrease towards the southwest, which is coupled with an increase in K-content of the erupted products (Molnár et al., 2022; Vougioukalakis, 1994). Two periods of lava dome building activity have been identified in the evolution of KV (6.5–4 Ma and 3–1.8 Ma; Janković et al., 1997; Kolios et al., 1980; Molnár et al., 2022). The majority of the erupted products have trachytic, trachydacitic, or trachyandesitic composition, with a high-K calc-alkaline affinity in the older (>4 Ma) lava domes, whereas the <3 Ma erupted products bear shoshonitic affinity (Molnár et al., 2022 and references therein). The volcanic system is surrounded by the extensional Mariovo, Tikveš and Almopia basins towards the northwest, northeast, and south, respectively, with thick basin-filling pyroclastic deposits present on all sites (Fig. 1). The Late-Miocene – Pleistocene successions of these basins are characterized by a predominantly lacustrine depositional environment, where the lake sediments (e.g., marl, travertine) are intercalated with lignite and fluvial deposits in addition to the volcaniclastics (Dumurdzanov et al., 2003; Steenbrink et al., 1999).

At least four large explosive eruptions were identified at ca. 5.8, 4.9, 4.1 and 2.5 Ma (Boev and Ivanova, 2024; Steenbrink et al., 1999;

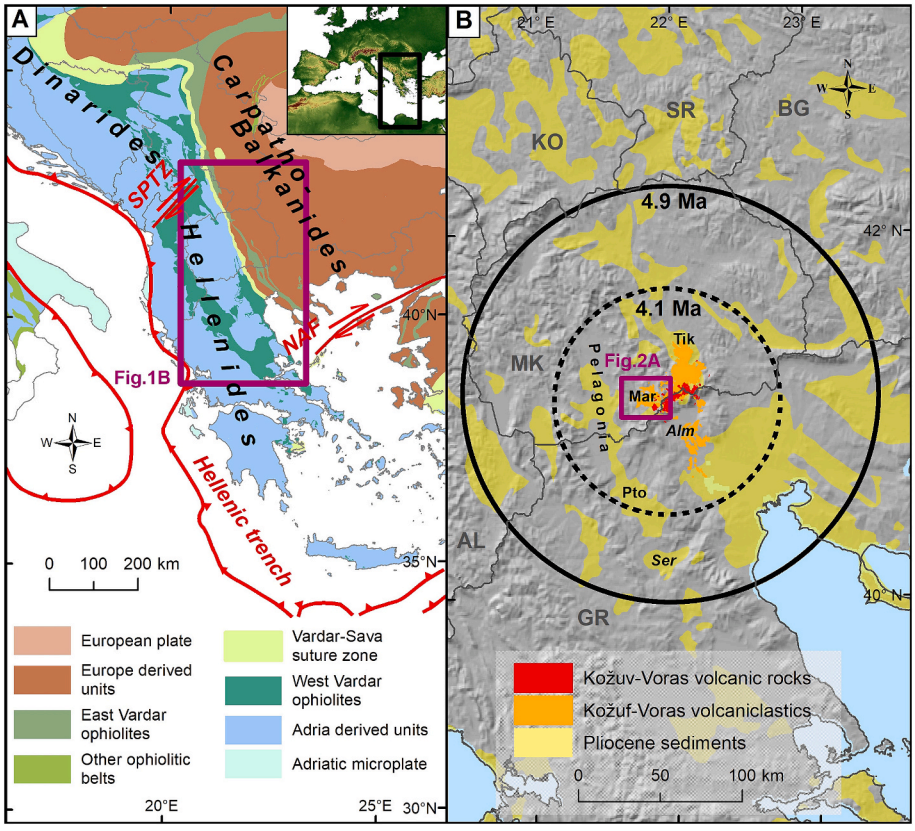

Fig. 1. Location of the study area. A: Geotectonic setting of SE Europe (modified after Schmid et al., 2020). SPTZ: Skutari-Peć transverse zone, NAF: North Anatolian Fault. B: Location of the Kožuf-Voras volcanic system in relation to basins with Pliocene sediments in the central parts of SE Europe. Estimated dispersal ranges for the 4.9 Ma and 4.1 Ma eruptions are indicated (based on Vougioukalakis, 2002). Mar – Mariovo basin, Tik – Tikveš basin, Pto – Ptolemais basin, Ser – Servia basin. Shaded relief based on digital elevation data from SRTM 1 Arc-Second Global dataset, https://doi.org/10.5066/F7PR7TFT.

Vougioukalakis, 2002). Volcanic ash layers up to 25 cm in thickness intercalated with lignite-marl successions were recognized in the neighboring Ptolemais-Servia basins, as well (e.g., Steenbrink et al., 1999, 2006). Estimates on the intensity of the explosive eruptions indicate that ashes could have reached the Gulf of Thessaloniki (located ca. 150 km SE from KV; Fig. 1; Vougioukalakis, 2002).

While there is some data on the tephra layers in the basins located to the NE (Tikveš basin) and S (Almopia basin) of KV (e.g., Boev and Ivanova, 2024; Vougioukalakis, 2002), not much data is available on the volcanoclastic occurrences in the Mariovo basin, located to the west of KV (Dumurdzanov et al., 2003). Recently, Molnár et al. (2023) identified a 2.8 Ma, ca. 3 m thick, massive lapilli tuff layer in the Mariovo basin related to an explosive eruption of the rhyolitic Šumovit Greben, which is the westernmost KV lava dome. However, the other occurrences have not yet been studied, even though these could provide additional key stratigraphic horizons.

3. Methods

We conducted two field campaigns in spring 2021 and 2022 to accurately map the volcanoclastic deposits and collect suitable samples from every mapped unit to unravel the explosive volcanic activity in the Mariovo basin. During the field campaigns, ten outcrops were sampled by hand-picking pumices, scoria, and lava rocks, or by collecting bulk samples from the volcaniclastic layers (see Table 1 for details). Sampling locations (Fig. 2), detailed description of the geological profiles, and detailed analytical procedures are presented in the Supplementary Materials (SM1, SM2, SM3).

3.1. Petrography, whole-rock geochemistry and glass geochemistry

Petrographic analyses of the studied samples was performed with a petrographic microscope (Olympus BX53 equipped with Olympus DP23 camera) at the HUN-REN Institute for Nuclear Research (ATOMKI, Debrecen, Hungary).

Whole-rock major and trace element geochemical composition were analyzed at AcmeLabs (Vancouver, Canada; http://acmelab.com), where the major and minor elements were determined by ICP-OES, and trace elements were analyzed by ICP-MS following a lithium-borate fusion and dilution in acid.

The glasses represent matrix glass from the sampled pumice and scoria clasts, which were crushed and sieved to the 125–250 μm fraction. The glasses were analyzed at GEOMAR (Kiel, Germany) using wavelength dispersive JEOL JXA 8200 electron microprobe. Microprobe setup and data on reference materials obtained in the course of this study are given in SM2. More analytical details and data on long-term reproducibility of reference materials are provided in review papers by Ponomareva et al. (2017) and Portnyagin et al. (2020).

Trace element analyses of single glass shards were obtained by laser-ablation inductively-coupled plasma mass-spectrometry (LA-ICP-MS) at the Institute of Geosciences, Christian-Albrecht-University of Kiel, Germany using a QQQ-ICP-MS Agilent 8900 and a Coherent GeoLas ArF 193 nm Excimer laser ablation system. The analyses were performed using laser density of 5 J cm^{-2}, a repetition rate of 10 Hz, and a 24 μm ablation craters. Details of the analytical protocol are reported in SM2.

3.2. $^{40}Ar/^{39}Ar$ dating

Sanidine crystals (250–500 μm) were separated from the lapilli tuff units (GR04, GR08d, PO02p, VI02) and the lava rocks (GR11, PO03) at ATOMKI for $^{40}Ar/^{39}Ar$ dating. Twenty fresh and transparent K-rich feldspars per sample were handpicked and irradiated in the Cd-lined core of the CLICIT facility at the Oregon State University TRIGA reactor for 2 h. Following irradiation, measurements were performed at the Laboratoire des Sciences du Climat et de l'Environnement (CEA, CNRS, France) dating facility. Gases of about 12 crystals per sample were individually extracted by fusion using a CO_2 laser and purified using 3 SAES getters. The five argon isotopes (i.e., ^{40}Ar, ^{39}Ar, ^{38}Ar, ^{37}Ar, and ^{36}Ar) were measured using a multi-collector NGX 600 mass spectrometer. Neutron fluence J factor (ranging from 0.00055580 ± 0.00000033 to 0.0005591 ± 0.000000335) was calculated using co-irradiated Alder Creek sanidine standard (ACs-2; 1.1891 Ma; Niespolo et al., 2017), according to the K total decay constant of Renne et al. (2011; $\lambda e.c. = (0.5757 \pm 0.016) \times 10^{-10}$ yr^{-1} and $\lambda\beta^{-} = (4.9548 \pm 0.013) \times 10^{-10}$ yr^{-1}). Discrimination is calculated using the $^{40}Ar/^{36}Ar$ ratio of 298.56 (Lee et al., 2006). Weighted mean age uncertainties including J uncertainty, were calculated using Isoplot 4.0 (Ludwig, 2012). Complete analytical data for each sample, along with a detailed description of the analytical procedures, are provided in the SM3.

Crystals with a low K/Ca ratio (probably plagioclase; present in samples GR11, PO02p and PO03) were excluded from the Kernel density estimates and the age calculation.

3.3. (U—Th)/He dating

The (U—Th)/He dating of zircons was performed at ETH Zurich (Switzerland). Euhedral zircons with widths >60 μm were selected. Zircons were packed in Nb foil, and the ^{4}He content of each grain was determined by outgassing with a diode laser at 1090 °C for 45 min and measuring the released gas on a sector-field noble gas MS in static vacuum. Outgassed zircons were transferred into Teflon vials, isotopically spiked with a mixed U—Th solution, and dissolved. U and Th

Table 1
Summary of the studied samples.

Valley	Outcrop	Pyroclastic layers	Sampled material (and specific layers)	Methods	Age (Ma)	Lithofacies (of the sampled layer)	Interpretation	Profile
Gradeška river drainage	GR04	GR04	pumice	age, WR, glass, Sr-Nd	3.93 ± 0.04	massive lapilli tuff	pyroclastic flow	F
	GR07	GR07b-g	bulk (GR07b, c, g)	WR	n.d.	stratified tuff-lapilli tuff	pyroclastic flow	D
	GR08	GR08c-g	pumice (GR08d)	age, WR, glass, Sr-Nd	2.66 ± 0.03	massive lapilli tuff with pumice lenses	pyroclastic flow and fall-out	D
	GR09	GR09	scoria	WR, glass	n.d.	scoria agglomerate	pyroclastic flow	D
	GR11	GR11	lava rock	age, WR, glass, Sr-Nd	2.56 ± 0.02	lithic breccia	block-and-ash flow	D
Buturica river drainage	PO02	PO02p	pumice	age, WR, glass	3.83 ± 0.03	massive lapilli tuff	pyroclastic flow	C
	PO03	PO03	lava rock	age, WR, glass, Sr-Nd	3.61 ± 0.02	lithic breccia	block-and-ash flow	C
	VI02	VI02	pumice	age, WR, glass	3.73 ± 0.04	massive lapilli	phreatomagmatic ash or fall-out	A
	RA01	RA01	scoria	WR, glass	n.d.	scoria agglomerate	pyroclastic flow	B
	RA02	RA02	pumice	WR, glass	n.d.	massive lapilli tuff	pyroclastic flow	B

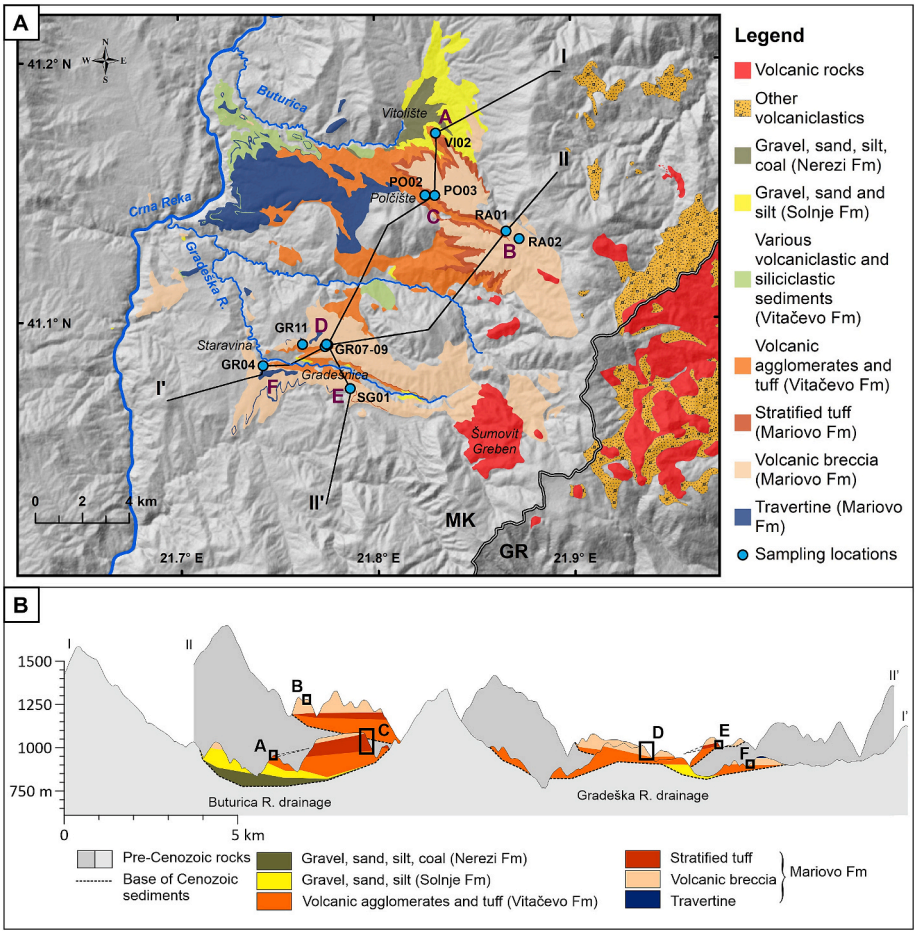

Fig. 2. Lithological map of Mariovo basin sediments and its relation to the Kožuf-Voras volcanic system (A) and cross sections of the studied units with 5× vertical exaggeration (B). Labels A-F on the map and cross-sections refer to the studied profiles (presented in detail in Fig. 3).

concentrations were determined via measurement of U and Th isotope ratios on a single-collector SF-ICP-MS (Element XR). Two zircons from the Fish Canyon Tuff were processed with our samples but one failed and the remaining zircon gave a (U—Th)/He age of 28.2 ± 0.2 Ma that is consistent with an eruption age of 28.2–28.0 Ma (Boehnke and Harrison, 2014).

3.4. Sr and Nd radiogenic isotopes

The Sr and Nd isotope analyses were carried out at the Istituto di Geoscienze e Georisorse – CNR of Pisa (Italy) on four samples (GR04, GR08d, GR11, PO03), using a ThermoFisher Neptune Plus MC-ICP-MS, in 2% HNO_3 solution containing 20–200 $ng*g^{-1}$ of analyte, after leaching for 30 min with strong ultrapure HCl (6.6 N) to remove secondary phases. Sr and Nd were extracted from the matrix in class 100 clean rooms, after conventional cation-ion exchange techniques. The analytical accuracy and long-term external reproducibility for $^{87}Sr/^{86}Sr$ of reference material NIST SRM 987 was 0.710251 ± 12 (n = 38), and for $^{143}Nd/^{144}Nd$ of reference material J-Ndi-1 was 0.512098 ± 5 (n = 17). Full analytical details are given in Agostini et al. (2022).

4. Results

4.1. Characterization of Mariovo basin volcaniclastic deposits

The sedimentary successions in the eastern parts of Mariovo basin are characterized by primary and redeposited volcaniclastic layers, which are intercalated with travertine and tufa, conglomerate and breccia layers (Fig. 2) representing a lake/fluvial environment, where the deposition was interrupted by intermittent volcanic eruptions (Dumurdzanov et al., 2003). The studied profiles form valley-filling volcano-sedimentary successions. The southern, W-E trending one, is located in the Gradeška river drainage, near Gradešnica village, whereas the northern, NW-SE trending one, is located in the upstream parts of Buturica valley, between Polčište and Vitolište villages (Fig. 2). Geological mapping and previous studies in the area defined two main units, consisting of quartz latite agglomerate and tuff at the bottom and quartz latite breccia at the top of the succession, with the same stratigraphy assumed for both valleys (e.g., Dumurdzanov et al., 2003). Here, we summarize the main characteristics of the studied profiles, together with their stratigraphic columns (Fig. 3, Table 1), whereas the detailed descriptions of the profiles are presented in SM1.

The volcaniclastic layers occur as primary (e.g., different types of lapilli tuff) and redeposited layers (slope deposits/debris flows). Profiles D and F are located in the Gradeška river drainage, and the primary layers are the following (in stratigraphic order). Profile F: GR04 (Figs. 2, 3), a ca. 1 m thick, massive lapilli tuff layer (mLT) of unsorted, non-welded and matrix-supported layer containing crystal-poor pumices and lithic clasts, topped by a ca. 1.5 m thick, matrix-supported, unsorted, massive lithic breccia (mlBr) layer with scarce pumices. The base of the unit is not visible, whereas the massive lithic breccia layer is followed by a travertine layer. Profile D: GR07, a ca. 1.1 m thick, slightly altered, stratified tuff-lapilli tuff (sT-sLT), which is deposited on and topped by travertine layers. It is followed by a slope deposit (breccia) with clasts of various origins (volcanic and crystalline basement), a travertine layer and a conglomerate layer. This is the base of the next

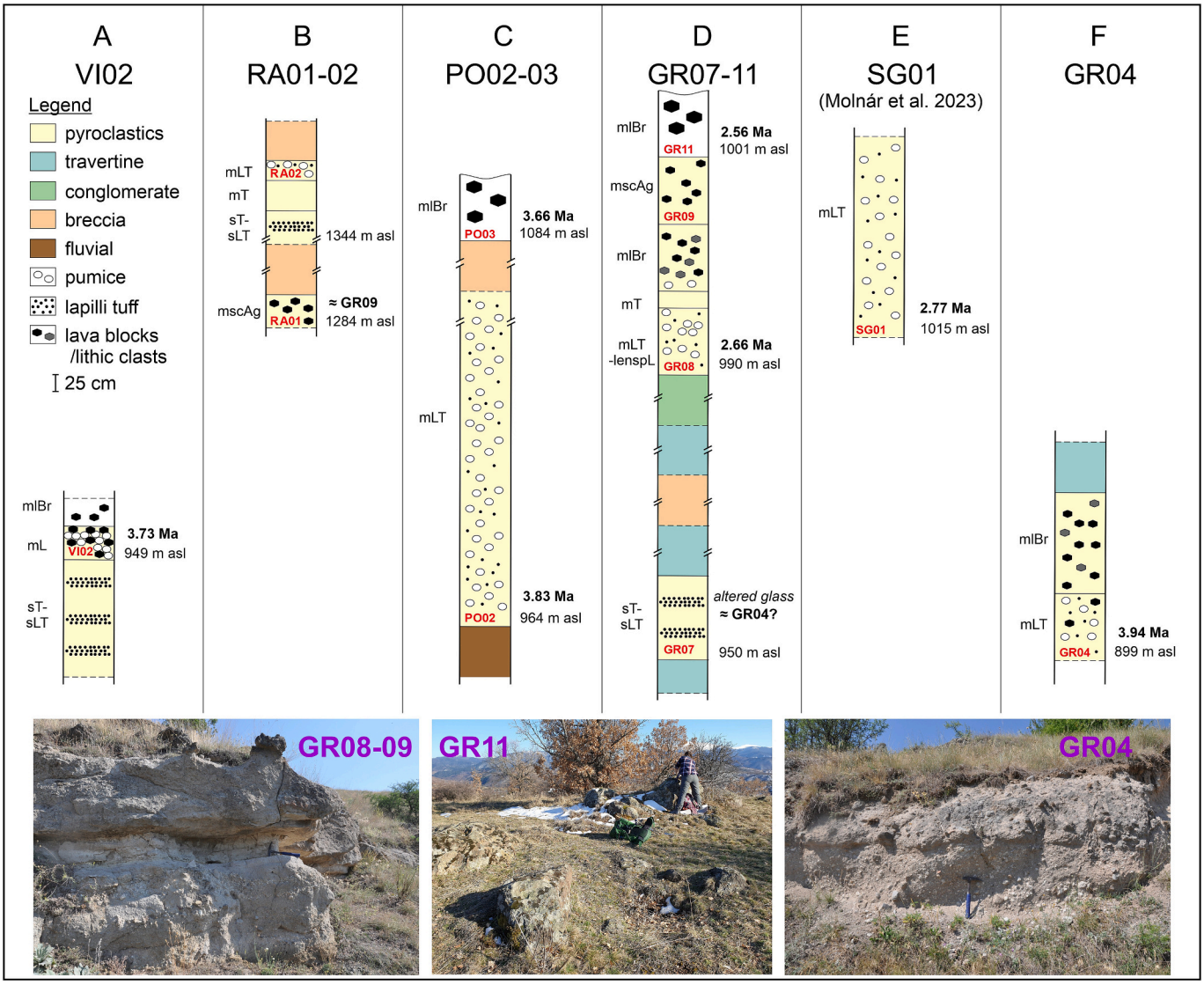

Fig. 3. Stratigraphic profiles of the volcaniclastic layers in the Mariovo basin and field photos of selected sites (additional field photos are available in SM1). Labels A-F mark their position on the lithological map (Fig. 2). Details of the pyroclastic layers are described in the text. White mlBr units mark lack of matrix. Each facies are named according to the pyroclastic lithofacies nomenclature of Branney and Kokelaar (2002).

primary layers of GR08, GR09 and GR11, which represent a continuous pyroclastic sequence with no sedimentary units or visible hiatus in between them (Fig. 3). GR08 is a ca. 2.5 m thick unit, which is composed of a massive lapilli tuff layer with pumice lenses (up to 1 m; mLT-lenspL), a massive tuff (−lapilli tuff) layer (ca. 25 cm; mT) and a massive lithic breccia layer (ca. 1 m; mlBr) with scarce pumices (Figs. 2, 3). It is followed by a scoria agglomerate unit (GR09; mscAg), where the matrix is eroded towards the top of the sequence, and a lithic breccia of monomict, poorly sorted blocks and boulders up to 2 m in diameter (GR11; mlBr), where no matrix is present (Figs. 2, 3).

Profiles A, B, and C are located in the Buturica river drainage, and the primary deposits are the following (in stratigraphic order). Profile C: PO02p, a ca. 5 m thick, unsorted, non-welded, matrix-supported massive lapilli tuff layer (mLT) containing crystal-poor pumices and scarce lithic clasts (Figs. 2, 3), which is deposited on a fluvial succession. PO02p is followed by a slope breccia with clasts of various origin (volcanic and crystalline basement), which is followed by PO03, a lithic breccia/agglomerate of monomict, poorly sorted blocks and boulders up to 2 m in diameter (PO03, mlBr) with completely eroded matrix (Figs. 2, 3), similar to GR11. Profile A: a ca. 2 m thick stratified tuff-lapilli tuff (sT-sLT), topped by a ca. 0.5 m thick, clast-supported massive lapilli layer with pumices up to 5 cm, and smaller, homogeneous lithic clasts (VI02, mL) (Figs. 2, 3). Profile B: a matrix-dominated scoria agglomerate unit (RA01, mscAg) (Figs. 2, 3) with scoria clasts, which resembles the GR09 unit. This is followed by a slope deposit, and a ca. 1.5 m thick section of stratified lapilli tuff (sLT, ca. 50 cm), massive tuff (mT, ca. 40 cm) and massive lapilli tuff (RA02, mLT, ca. 40 cm) with pumice clasts up to 5 cm (Figs. 2, 3).

4.2. Eruption ages of the tephra layers

Single-crystal sanidine $^{40}Ar/^{39}Ar$ and zircon (U—Th)/He dating revealed at least 7 eruption events over 4.0–2.5 Ma (Fig. 4). Detailed age data for individual crystals from each sample and method are presented in SM3. Weighted mean $^{40}Ar/^{39}Ar$ age uncertainties are reported at 2σ, including J uncertainty, calculated using Isoplot 4.0 (Ludwig, 2012). Xenocrysts present in samples GR11, PO03, and PO02p were not included in the weighted mean age calculation but are presented in Fig. 3. The main population of crystals in each sample is interpreted as juvenile, i.e., the age of deposition of the volcanic units. Eruption ages determined by sanidine $^{40}Ar/^{39}Ar$ and zircon (U—Th)/He methods overlap within uncertainty (SM3). In case of those samples, where both

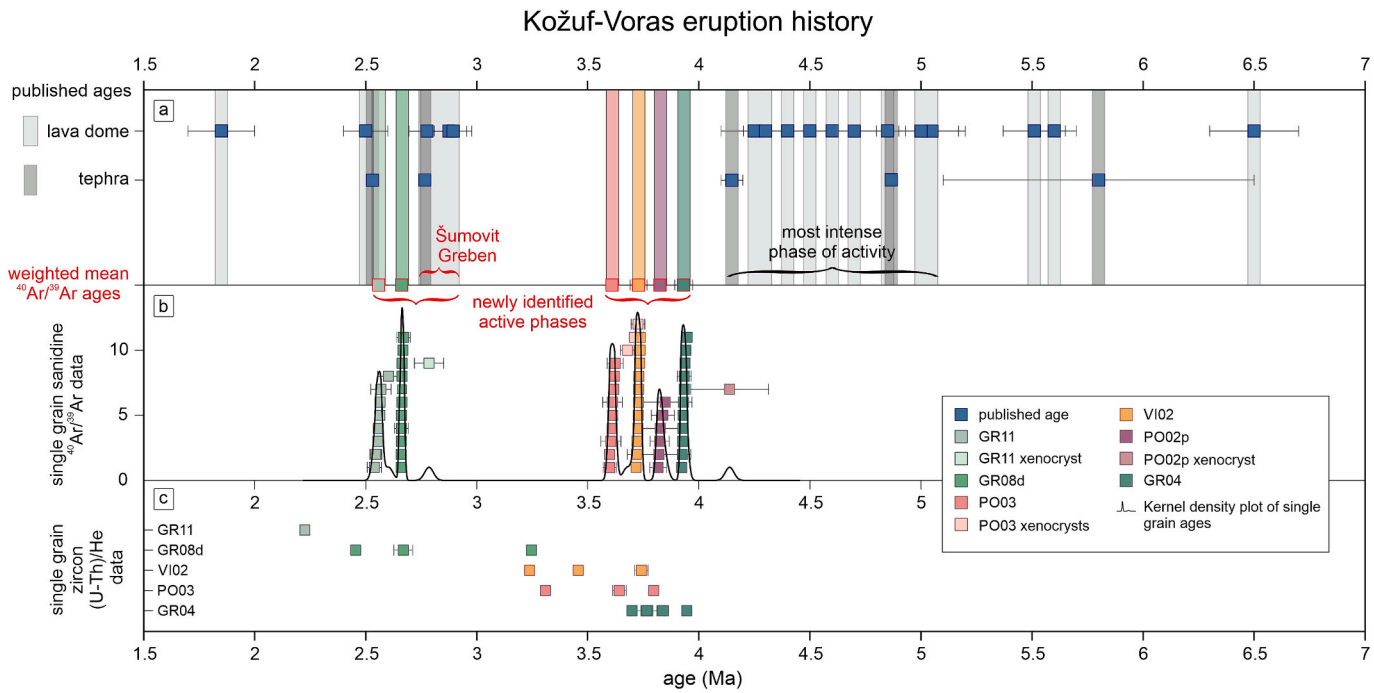

Fig. 4. Kožuf-Voras eruption history. (a) Lava dome and tephra ages, including published data, are shown emphasizing the previously (black) and newly (red) identified most active phases (Boev and Ivanova, 2024; Janković et al., 1997; Kolios et al., 1980; Molnár et al., 2022, 2023; Steenbrink et al., 1999; Vougioukalakis, 2002; this study). (b) Single-crystal sanidine $^{40}Ar/^{39}Ar$ ages with weighted means for each sample, together with their Kernel density plots. (c) Single grain zircon (U—Th)/He ages. (For interpretation of the references to colour in this figure legend, the reader is referred to the web version of this article.)

methods were applied, single grain data spans from 2.66 to 2.67 Ma and 2.45–3.24 Ma (GR08d); 3.60–3.73 Ma and 3.31–3.74 Ma (PO03), 3.72–3.74 Ma and 3.24–3.80 Ma (VI02), and 3.92–3.95 Ma and 3.70–3.94 Ma (GR04) for the $^{40}Ar/^{39}Ar$ and the (U—Th)/He methods, respectively (Fig. 4). Due to the larger number of measured crystals (hence, smaller uncertainties), only the sanidine $^{40}Ar/^{39}Ar$ ages are discussed further (Table 1).

Based on the obtained ages, an older and a younger age group can be differentiated (Fig. 4). The older group spans from 4 Ma to 3.5 Ma with samples GR04 (3.93 ± 0.04 Ma), PO02p (3.83 ± 0.03 Ma), VI02 (3.73 ± 0.04 Ma) and PO03 (3.61 ± 0.02 Ma). The younger group is represented by samples GR08d (2.66 ± 0.03 Ma) and GR11 (2.56 ± 0.02 Ma) in spanning the age range from 3 Ma to 2.5 Ma. This latter closely follows the extrusive and explosive activity at the rhyolitic Šumovit Greben lava dome (Fig. 4; 2.9–2.8 Ma; Molnár et al., 2022, 2023), and overlaps with the youngest recognized explosive eruption on the southern site of KV (2.53 ± 0.03 Ma; Vougioukalakis, 2002).

4.3. Petrography and whole-rock geochemistry

The studied pumices, scoriae and lava blocks show very similar mineral composition of clinopyroxene, biotite, plagioclase and sanidine as the main phenocrysts, and zircon, apatite and Fe—Ti oxides as the most abundant accessory phases (Fig. 5). The scoria samples have vitrophyric textures, whereas the lava rock samples exhibit differences in crystallinity of the groundmass, GR11 is dominantly glassy (hyalopilitic texture), whereas PO03 is more crystalline. Thicker biotite reaction/breakdown rims are also more characteristic of the latter sample. Disequilibrium textures are often observed in all the samples including sieved inner rims and/or cores in plagioclase, complex zonation of clinopyroxene together with the presence of mafic crystal agglomerates containing primarily plagioclase, clinopyroxene and Fe—Ti oxide (Fig. 5). The tuff samples from GR07 unit contain several non-volcanic xenocrysts and xenoliths (e.g., quartz, feldspar, mica; clasts from basement sandstone, mica schist and granulite) in addition to plagioclase, biotite and clinopyroxene.

Glass shards from the pumice and scoriae samples show distinct characteristics (Fig. 5; described in detail in SM1). GR04 pumice contains dominantly crystal fragments with minor juvenile vesicular vitric shards (Fig. 5e), whereas GR08d pumice is characterized by mainly juvenile, highly vesicular vitric shards with crystal fragments (Fig. 5h). Blocky clasts with unconnected pores are present in the GR09 scoria. The vesicularity of the clasts varies from dense to highly vesicular with larger bubbles. PO02p pumice contains dominantly juvenile, vesicular glass with irregular shape and generally high porosity. VI02 pumice is characterized by juvenile shards and cored ash pellets containing blocky or elongated glass at their core (Fig. 5g). RA01 scoria sample is composed of crystal fragments, and irregular to elongated shape, high porosity shards with rounded bubbles. RA02 pumice contains minor juvenile glass of irregular shape with moderate to high vesicularity.

The studied samples are basaltic trachyandesite to trachyte based on the whole rock geochemical composition / total-alkali silica (TAS) classification. However, some of the samples show signs of alteration (e.g., GR07b, c, g; RA02 with LOI > 5 wt%), in which case the major element composition might be affected and were excluded from further interpretation. In the GR07 samples, the trace element composition cannot be entirely conclusive either due to the presence of non-volcanic xenocrysts. The studied samples belong to the shoshonitic series (Peccerillo and Taylor, 1976); SiO_2 = 53.8–60.4 wt%, K_2O = 4.3–6.2 wt %; recalculated anhydrous; SM2) and to group C and D based on the hierarchical cluster analyses of Molnár et al. (2022) (Fig. 6). Trace element composition falls in the range of the KV, and shows enrichment in LIL elements, U and Th relative to some HFS elements (Nb, Ti) exhibiting slight negative Eu-anomaly (0.68–0.90 Eu/Eu*). The $^{87}Sr/^{86}Sr$ and $^{143}Nd/^{144}Nd$ isotopic ratios of the studied samples fall into the enriched/crustal quadrant of the classical Sr—Nd isotopic diagram, ranging from 0.70864 to 0.71004 and from 0.51223 to 0.51234, respectively. The studied samples follow a trend similar to that of other KV samples (Fig. 6), characterized by a rough positive correlation between $^{87}Sr/^{86}Sr$ and SiO_2 content. These differences testify evolution in

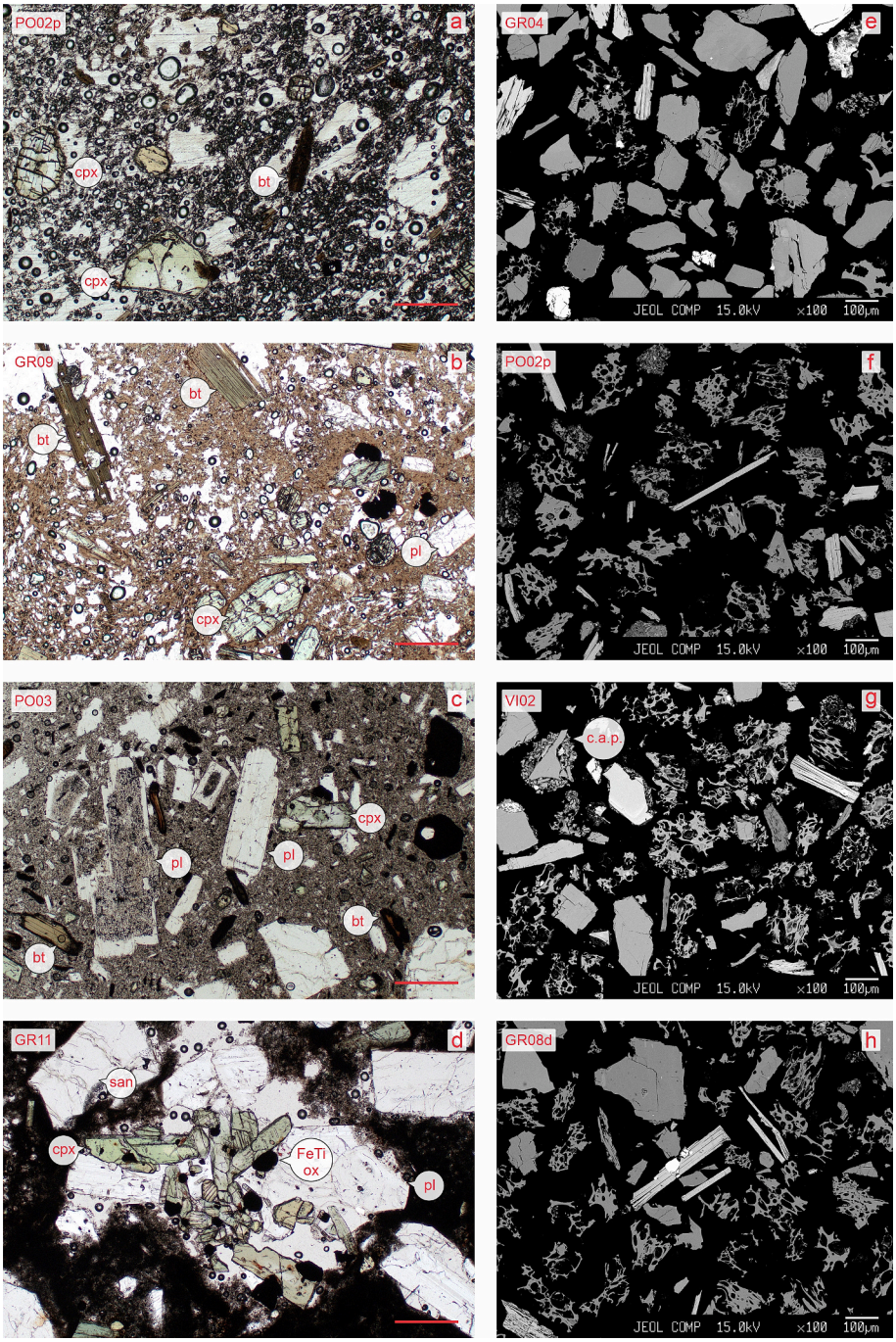

Fig. 5. Petrographic microscopic photos (1 N) of selected pumice (a), scoria (b) and lava rock samples (c-d); and BSE images of selected pumice samples (e-h; 125–250 µm fraction). The scale is 500 µm unless otherwise marked. Complex zonation of clinopyroxene (a, c), sieved plagioclase (c) and mafic crystal agglomerate (d) are characteristic of the samples. cpx: clinopyroxene, bt: biotite, pl: plagioclase, san: sanidine, Fe—Ti ox: Fe—Ti oxide, c.a.p: cored ash pellet.

an open system, i.e., with significant crustal assimilation during fractional crystallization of magmas. In particular, the GR08d pumice and GR11 lava rock, which slightly differ from the other KV samples for their higher $^{87}Sr/^{86}Sr$ and lower $^{143}Nd/^{144}Nd$ ratios, a more enriched source or a stronger amount of crustal contamination should be invoked.

4.4. Glass geochemistry

Major and trace element composition of glass shards from pumice samples GR04, GR08d, PO02p, VI02, RA02, and scoria samples GR09, RA01 are presented in SM2 and plotted in Fig. 7. As samples from the GR07 profile contained only altered glass shards, these were not included in the analyses. The glass composition is more uniform and shows a more evolved character compared to the whole-rock composition of the same samples. The samples exhibit trachytic to rhyolitic (GR04, VI02) composition with SiO_2 = 62.0–73.0 wt%, Al_2O_3 = 14.7–19.6 wt%, and total alkali content of 7.0–13.4 wt% (recalculated anhydrous). Except for VI02, which presents a broader range of composition (e.g., SiO_2 = 66.6–73.0 wt%) possibly reflecting the different extent of fractionation of the same melt, each sample has a distinct, narrow range of composition (Fig. 7). Samples RA01 and GR09, and RA02 and GR08d have slightly overlapping composition based on their K_2O, CaO and SiO_2 content. Similar to the whole-rock composition, each sample shows enrichment of LIL elements except for Ba relative to

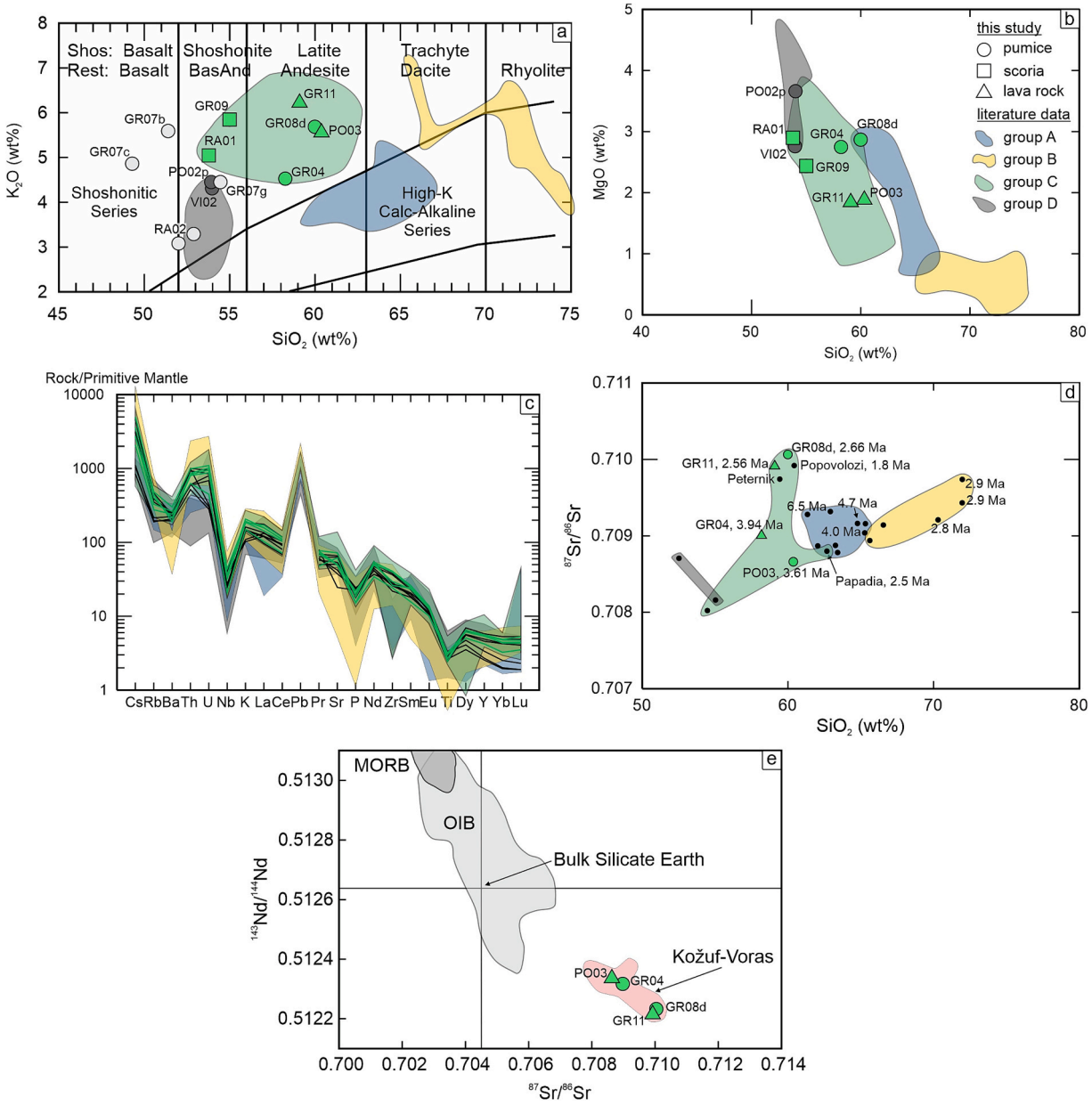

Fig. 6. Whole rock geochemical data of the studied samples compared to previously published results from the Kožuf-Voras volcanic system (summarized in Molnár et al., 2022). The groups A (blue), B (yellow), C (green) and D (grey) are updated from the hierarchical cluster analyses (Molnár et al., 2022). a: SiO_2 (wt%) vs. K_2O (wt%) modified after Peccerillo and Taylor (1976), where the pale grey circles indicate altered samples (not included in the other diagrams). b: SiO_2 (wt%) vs. MgO (wt%). c: trace element diagram normalized to primitive mantle (Sun and McDonough, 1989). d: $^{87}Sr/^{86}Sr$ ratio vs SiO_2 (wt%) with ages from literature data and names of the relevant lava domes presented. e: $^{87}Sr/^{86}Sr$ vs. $^{143}Nd/^{144}Nd$ ratios (Bulk Silicate Earth value, MORB and OIB fields are from Zindler and Hart, 1986). (For interpretation of the references to colour in this figure legend, the reader is referred to the web version of this article.)

the primitive mantle composition (Sun and McDonough, 1989). Nb, P, and Ti depletions are present in all the samples, with the highest expression in VI02 and GR04 (the two with rhyolitic composition). They also show a slight depletion in Sr and the largest depletion in Ba content, together with higher negative Eu-anomalies (average Eu/Eu* of 0.50 versus 0.77 in the other samples; Fig. 7). These samples, together with GR08d display elevated Rb/Sr ratios, which is consistent with plagioclase accumulation before the eruption (i.e., lower Eu/Eu* values; e.g., Cooper et al., 2016).

5. Discussion

5.1. Lithostratigraphic constraints and basin evolution

Combining geochronological and geochemical data with literature data, seven pyroclastic units can be differentiated in the 4.0–2.5 Ma period. This interval (except for the recent recognition of Šumovit Greben lava dome; Molnár et al., 2022, 2023) was considered as an inactive phase in the lifetime of Kožuf-Voras volcanic system as most of the recognized lava dome forming activity and explosive eruptions took place in the 5.0–4.2 Ma period (Fig. 4). While previous studies could not resolve differences in the stratigraphic record in the Mariovo basin, our findings show a complex eruptive history and magma generation for this area. High-precision sanidine $^{40}Ar/^{39}Ar$ ages (with uncertainties of

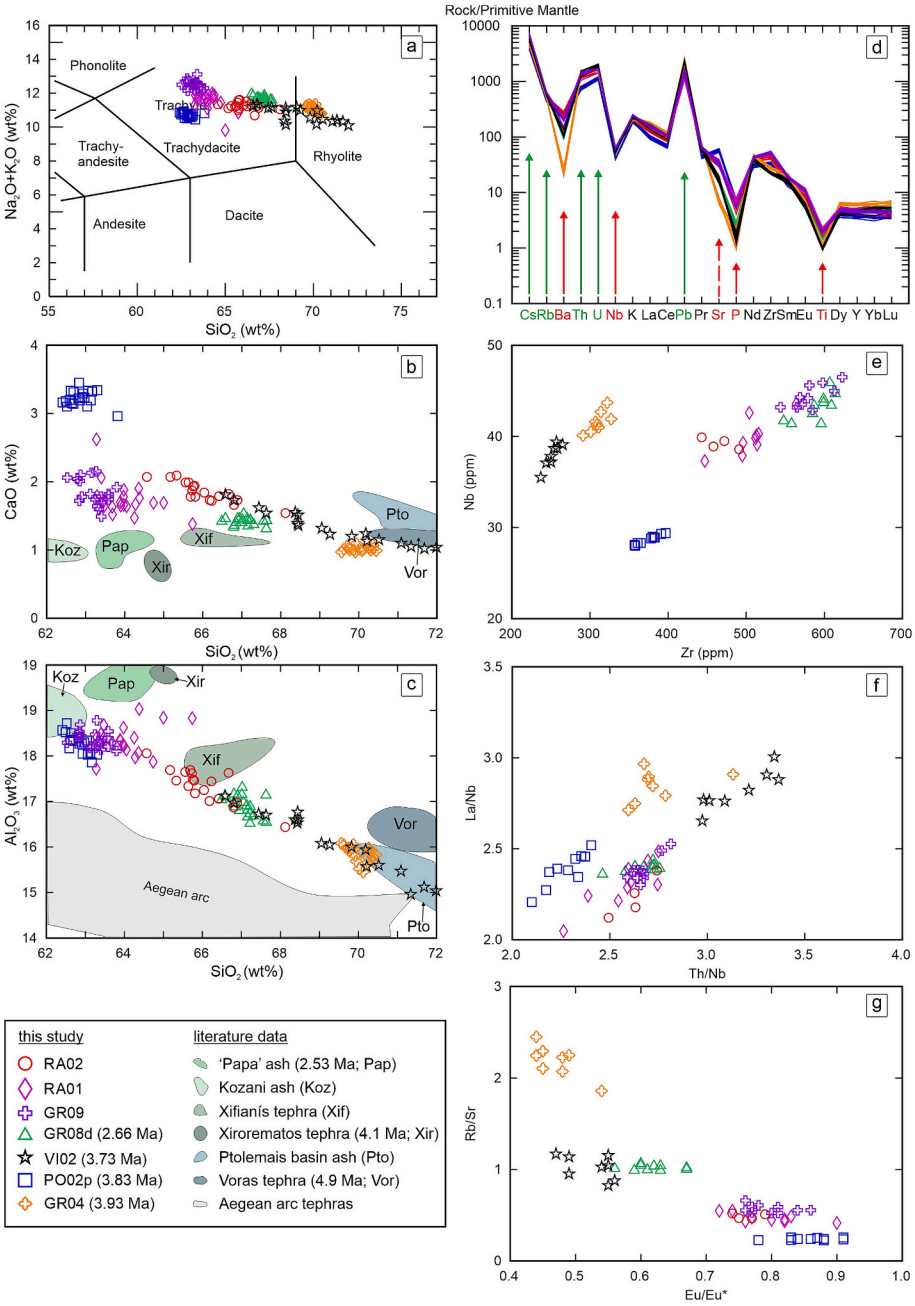

Fig. 7. Glass geochemical data of the studied samples. Major element composition is compared (b, c) to available glass data from other KV tephras (Vougioukalakis, 2002) and the Aegean volcanic arc (https://georoc.eu/).

0.02–0.04 Ma, <1% at 2σ) allow the distinction of several eruptive layers, emplaced in close succession, at intervals of ca. 100 ka.

The profiles in the Gradeška river drainage cover the longest interval of volcano-sedimentary succession starting with the 3.93 ± 0.04 Ma massive lapilli tuff layer (GR04) and finishing with the 2.56 ± 0.01 Ma lithic breccia (GR11; Fig. 3). Although there are no age or reliable geochemical data for the GR07 stratified tuff-lapilli tuff layer due to its alteration and the presence of xenocrysts, based on its stratigraphic position and elevation, we assume it might be correlated with the GR04 massive lapilli tuff (3.93 ± 0.04 Ma). Even though their lithofacies differ, the layers may be interpreted as two lithofacies of an ignimbrite depositing in the valley (GR04) and over topographic highs (GR07; e.g., Brown and Andrews, 2015). It is followed by a sedimentary succession spanning a ca. 1.3 Ma interval, which well represents the dynamics of the 'Mariovo lake'. The first post-volcanic layers were deposited in a fluvial or lacustrine environment (tufa and travertine), followed by slope breccia consisting mainly of clasts from nearby lava domes but also from the crystalline bedrock (subaerial). Subsequently, the depositional environment changed to lacustrine (travertine), then to fluvial (conglomerate) before the next volcanic, explosive phase (GR08). The base of the GR08 might have been deposited still in a subaqueous environment (close to the shore, e.g., Manville, 2001). The top of the profile shows another gap in volcanic activity based solely on ages (GR08 and GR11; 2.66–2.56 Ma). However, the volcanic succession is continuous (Fig. 3) with no sign of erosion, redeposition, or intermittent sedimentary layers. Therefore, we can assume ongoing volcanic activity during this interval with at least five eruptions occurring uninterruptedly (or shortly after each other). The top layer of the sequence (GR11; 2.56 ± 0.01 Ma) is the youngest unit in the newly recognized 'younger sequence'.

The studied profiles near the Polčište-Vitolište villages do not show intercalations with travertine; however, a large travertine deposit is present downstream along the Buturica drainage (Fig. 2). PO02p massive lapilli tuff (3.83 ± 0.03 Ma) is deposited on a sedimentary succession. It is overlain by a slope breccia containing mixed lava rock and bedrock clasts and followed by the PO03 lithic breccia (3.61 ± 0.02 Ma), the youngest unit in the newly recognized 'older sequence'. VI02 massive lapilli layer formed within the gap of PO02p and PO03, at 3.73 ± 0.04 Ma. Due to its close vicinity to the Polčište succession, the VI02 unit might be also present in the top section of the PO02p unit; however, it cannot be excluded that the consecutive pyroclastic density currents were focused in the distinct valleys, and these units do not intercalate with each other.

Further southeast, along the ridge from Vitolište, two more primary pyroclastic units can be found, RA01 and RA02 (Fig. 2). Although there are no age constraints for these layers, the RA01 scoria agglomerate unit resembles the GR09 unit in its lithofacies, petrographic characteristics and glass geochemical composition (Fig. 7) implying these layers could be correlated to each other as eruptions in the 2.66–2.56 Ma period. The RA02 unit of stratified lapilli tuff, massive tuff and massive lapilli tuff is not a direct continuation of RA01, as the two units are separated by a (slope) breccia (Fig. 3). However, their glass geochemical data show close similarities to each other (Fig. 7) therefore, it is likely that RA02 is also part of the younger sequence.

Lithic breccias topping the Gradešnica and Polčište profiles have different eruption ages (2.56 ± 0.01 Ma and 3.61 ± 0.02 Ma, respectively) and geochemistry. However, they share similar stratigraphic features. Both units (GR11 and PO03) appear as a sheet of poorly sorted, large blocks and boulders (up to 5 m in diameter) with homogeneous composition on a low-angle slope. Even though no matrix is present in either unit, they most likely represent sheet facies of block-and-ash flow deposits similar to those described during the 1998 Merapi eruption (Schwarzkopf et al., 2005). The matrix (ash), present at the time of deposition was most likely eroded since then. Although no lava dome is identified in their close vicinity, primary block-and-ash flow deposits can be found even up to 10 km distance source (e.g., Mt. Taranaki; Platz et al., 2007); with a usual runout distance of around 5 km (e.g., Merapi, Soufriere; Sulpizio et al., 2010), which is a similar distance to the closest lava domes in the area (Fig. 8). In case of GR11 unit, further redeposition e.g., by lahar transportation can be inferred as similar blocks and boulders can be found up to 5–10 km in distance from the GR11 sampling site. An alternative explanation could be that both PO03 and GR11 units are remnants of a lava dome or a lava flow. However, there is no topographic height at either of the locations to support the lava dome hypothesis, and the closest lava domes are too far away to produce continuous lava flows at such a distance due to the higher viscosity (e.g., Walker, 1973).

The pyroclastic layers are, in most cases, valley-filling pyroclastic density current deposits. Still, as lithic breccias cover the sequences, most of the profiles are located on present-day topographic highs. This provides an opportunity to estimate cumulative valley incision rates for the past ca. 2.56 and 3.61 million years at Gradešnica and Polčište sites, respectively. The relative elevation of the pyroclastic layer above the current river talweg is 140 m at Polčište and 120 m at Gradešnica, with estimated minimum cumulative incision rates (i.e., averaged over the entire timespan) of 0.04 m/ka and 0.05 m/ka, respectively (Fig. S3 in

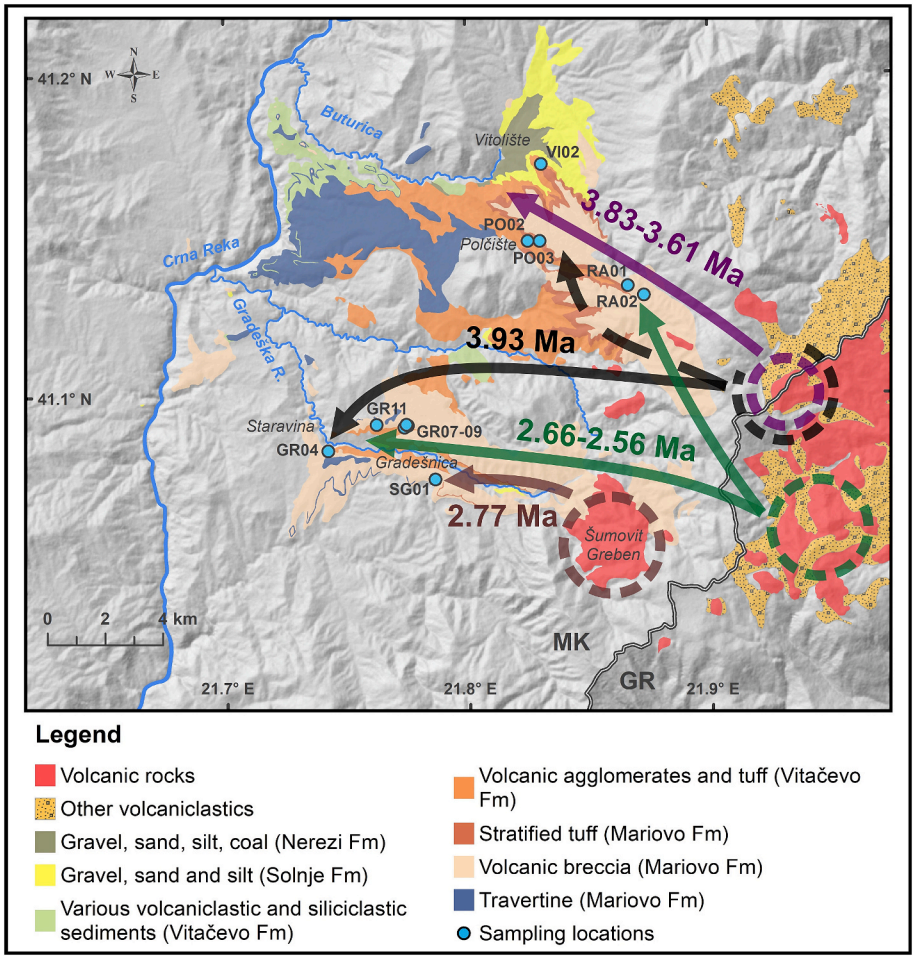

Fig. 8. Timing of the volcanic eruptions and interpreted source areas for Mariovo basin volcaniclastics.

SM1). The obtained values are comparable to estimated cumulative valley incision rates since the Early Pleistocene for the middle parts of the Buturica valley downstream from Polčište site (0.06 m/ka), as well as at Kamenica Valley (0.04 m/ka) in the lower part of the Crna Reka drainiage (Temovski et al., 2024).

5.2. Possible eruption centers and types of eruptions

There is no clear correlation between the previously described (and dated) lava domes and the newly identified pyroclastic profiles, as no volcanic eruptions were identified in the 4.0–2.6 Ma period except for the rhyolitic Šumovit Greben, which shows both effusive and explosive activity. Both explosive and lava dome-building activity were recognized at ca. 2.5 Ma ('Papa ash' and Papadia lava dome; Kolios et al., 1980; Vougioukalakis, 2002; Fig. 4), which might correspond to the GR11 unit. However, as their whole rock and glass compositions differ significantly from those of GR11 lithic breccia, they must represent different eruptions. On the other hand, whole-rock composition and Sr—Nd isotopic data of the GR08 pumice and the GR11 lava rock show some similarities to the 1.8 Ma Popovolozi lava dome, which is the youngest center of the KV and the nearby Peternik lava dome, with no age data available (Figs. 6, 8) (Eleftheriadis et al., 2003; Kolios et al., 1980). Although Popovolozi can be excluded due to its younger age, according to the geochemical and isotopic fingerprinting of the GR08-GR11 samples, the source area of these units might be the Peternik lava dome or some of its neighboring lava domes (Fig. 8), for which no geochemical-isotope data are available in the literature at present. The whole-rock composition of the GR04 massive lapilli tuff unit shows similarities to the lava dome cluster located at the Macedonian-Greek border with preliminary ages marking a similar time for activity (ca. 4 Ma; Janka et al., 2024) implying as a possible source region for the 3.93 Ma eruption (Fig. 8). The pyroclastic flow deposits from the older sequence (4.0–3.5 Ma) are present in the Buturica valley in higher thickness, while eruption products from the younger sequence (3.0–2.5 Ma) are dominant in the Gradeška river drainage implying either a possible shift of location in the eruption centers and/or a change in topography defining the valleys, where the flows could run down.

Characteristic features of the pyroclastic layers (e.g., ratio and shape of the juvenile shards, bubble shape, porosity) can help to identify different types of eruptions and volcanic explosivity (e.g., Benet et al., 2021; Mueller et al., 2011; Trafton and Giachetti, 2021), whereas conduit processes and explosive to effusive transition can be recognized from the lava rocks (e.g., Hoult et al., 2024). The GR04 and PO02p massive lapilli tuffs are most likely deposited from pyroclastic flows. VI02 shows characteristics of a phreatomagmatic ash or fallout from a co-ignimbrite ash (i.e., the presence of cored ash pellets; e.g., Brown et al., 2010), whereas GR08d massive lapilli tuff might have deposited from a subplinian or a phreatomagmatic ash. Dense shards, unconnected pores and variable vesicularity of the GR09 scoria agglomerate imply different vent processes and degassing (e.g., Benet et al., 2021). The lithic breccias topping both profiles (Fig. 3) present different petrographic features implying different conduit processes before the eruptions, which can help to better understand the explosive-effusive transition (e.g., Hoult et al., 2024). The PO03 lithic breccia is characterized by crystalline, microlite-dominated groundmass, which, together with the presence of biotite breakdown rims suggests a conduit lining or filling event prior to the eruption, when the magma underwent some cooling and degassing, allowing microlite formation. The glassy groundmass of GR11 (which follows the GR09 scoria agglomerate) implies less residence time in the top part of the conduit. It can be interpreted as an early dome emplacement incorporated into the block-and-ash flow during a dome collapse. Here, the continuous pyroclastic sequence records the transition from the explosive to the more effusive style of volcanic activity over a short period (2.66 Ma–2.56 Ma), starting with massive lapilli tuff and tuff layers deposited from subplinian or phreatomagmatic explosive eruptions, and progressing to a dome-collapse related block-and-ash flow deposit. The transition of the eruptive style is also recorded by the gradual decrease in the water content (4.1 wt% → 2 wt% → 0.7 wt%; SM2) together with an increase in crystallinity (from vitrophyric to hyalopilitic texture) (e.g. Popa et al., 2021).

5.3. Magma generation

Erupted products derive from an overall similar magma source, i.e., they belong to the same petrogenetic association with shoshonitic geochemical affinity and share the same petrographical characters, with a paragenesis including clinopyroxene, biotite, plagioclase, and sanidine as the main phenocrysts. Although more detailed compositional data is needed to reveal its exact scale (e.g. MacDonald et al., 2024), the observed disequilibrium textures (e.g., complex zonation of clinopyroxene, presence of mafic crystal agglomerates; Fig. 5) imply multiple magma mixing events in a potentially trans-crustal magmatic plumbing system (e.g., Cashman et al., 2017).

Tephra deposits with well-defined stratigraphic order can help to track changes in composition through time (e.g., Brlek et al., 2024; Harmon et al., 2024; Perkins and Nash, 2002). Variation in glass composition between the eruptions might reflect the sequential evacuation of discrete melt-dominant bodies extracted from a mush zone (or different mush zones of a complex magma storage system) (e.g., Cooper et al., 2016; Wilson et al., 2021). Combining the whole rock composition of the two lithic breccias and the glass composition of the tephra layers, changes in the erupted composition can be traced through the 3.93–3.61 Ma (GR04, PO02p, VI02 and PO03 units) and the 2.66–2.56 Ma interval (GR08, GR09 and GR11 units) as these units have both well-defined ages and glass compositions (GR09 has no age but it is bounded between the GR08 and GR11 units).

The older sequence (3.93–3.73 Ma) displays rhyolitic (GR04, VI02) and trachytic (PO02p) composition (Fig. 7). Except for the VI02 major element composition, which reflects the different extent of fractionation within the same melt, no within-sample compositional heterogeneity is present, implying the evacuation of discrete melt bodies as main mechanism. The strong Eu-anomaly in samples GR04 and VI02, coupled with Ba and Sr depletion reflects feldspar (plagioclase) crystallization before the eruption, in line with their low Eu/Eu* and high Rb/Sr ratios. In contrast, P and Ti depletion can be explained by the crystallization of apatite and Fe—Ti oxides in the magma storage system. Evacuation of a compositionally zoned magma body might be considered for GR04 and PO02p (assuming the same eruption center), however, their sharp differences in some High Field Strength Element, e.g., Nb and Zr content, as well as La/Nb, Th/Nb ratios, possibly reflect different source depletion. The trachytic PO02p is followed by the rhyolitic VI02, which could imply continuous fractional crystallization of the non-erupted melt during the PO02p eruption; however, these samples also display differences in their trace element characteristics (Fig. 7), suggesting that sequential evacuation of closely emplaced, multiple, discrete, melt-dominant bodies characterized the explosive eruptions during the older sequence.

The younger sequence (2.66–2.56 Ma) has a more homogenous trachytic composition (Fig. 7). The different Sr—Nd isotopic composition of these samples compared to the older sequence suggests different source regions for the magmas with a more enriched character, or markedly different evolutionary processes, characterized by much higher amount of crustal assimilation during magma evolution with respect to the older products. The major element content of these samples (GR08d, GR09, RA01, and RA02) implies different extents of fractionation within the same melt. The trace element composition does not show different source depletion (e.g., overlapping composition in La/Nb and Th/Nb ratios), and the higher Rb/Sr ratio of GR08d together with the low Eu/Eu* value, Ba, Sr, P and Ti depletion (Fig. 7) reflects plagioclase, apatite, and Fe—Ti oxide crystallization before the eruption. As GR08d is the oldest unit (2.66 Ma), which represents the more

evolved character, this younger sequence might represent a compositionally zoned single melt body (e.g., Chamberlain et al., 2015; Hildreth and Wilson, 2007), which evacuated during the 2.66–2.56 Ma period. This is also supported by the decrease in SiO_2 and the $^{87}Sr/^{86}Sr$ ratio in the younger unit (Fig. 6). Although no age constraints are available for samples RA01 and RA02, the petrological and geochemical characteristics of RA01 resemble those of the GR09 unit; therefore, they might be correlated.

5.4. Regional tephra comparison

Vougioukalakis (2002) described in detail the tephra occurrences on the Greek side of KV and their possible dispersion in the region, implying some of the eruptions could produce tephra reaching the Gulf of Thessaloniki, located about 150 km SE from KV (Fig. 1). The obtained ages from these layers reveal two larger eruptions at 4.9 Ma and 4.1 Ma within the most intense phase of activity in KV (and the 2.53 ± 0.03 Ma 'Papa' tephra), which do not overlap in age with the newly identified pyroclastic layers (Fig. 4). Available glass geochemical major element data also shows no overlap with the other KV tephra layers (some of them do not have any age constraints; Fig. 7). Therefore, the newly identified pyroclastic layers truly represent new explosive eruptions in the evolution of KV, and due to its different composition and precise age, new correlation opportunities for the region.

Pliocene sedimentary basins are widespread in the central parts of SE Europe (Fig. 1), and several contain lignite deposits that remain crucial to the industry in the region. Ash intercalations within these sedimentary layers frequently occur. One example is the Ptolemais basin, which was studied in detail to constrain its depositional cycles (e.g., Steenbrink et al., 1999, 2006). Although the youngest dated ash layer was 4.04 ± 0.04 Ma, at least four younger ash layers are marked in the profile (Steenbrink et al., 1999, 2006), which might be correlated to the explosive eruptions of the older sequence (4.0–3.5 Ma) of the Mariovo basin. Ash layers were also recognized within the lignite/sedimentary sequence in Bitola (Pelagonia) basin with no age constraints (Boev and Ilijovski, 2013), which might also be correlated with the tephra layers from the older sequence (especially GR04) based on their location and proposed stratigraphy. Exploratory drilling for coal took place around Polčište (in the Mariovo basin), identifying an older tephra layer than the PO02p unit, which might also be correlated either with the 3.93 Ma GR04 unit, the 4.1 Ma Xiroremátos tephra or the 4.9 Ma Voras tephra layers (Steenbrink et al., 1999; Vougioukalakis, 2002; this study).While the dispersion of the newly identified tephra unit is unknown, these findings imply that a similar dispersion can be assumed to what was proposed for the older explosive events (Fig. 1).

Located further to the south, volcanism along the still-active Hellenic trench/South Aegean arc overlaps in age with the KV volcanism (e.g., Pe-Piper and Piper, 2007; Vougioukalakis et al., 2019). However, based on the available glass geochemistry data, there is no overlap with the Aegean tephras (Fig. 7), making the KV tephras new potential marker layers to improve the tephrostratigraphic framework in the region. Holocene Italian tephras are recognized in the area due to the present-day wind direction, traveling at least 400–600 km (e.g., Lake Ohrid; Wagner et al., 2019). However, Italian sources for the tephra layers in the Mariovo basin can be excluded, as the identified lithofacies imply much closer eruption centers. Although past (4–2.5 Ma) wind directions are not known, assuming similar conditions to present-day, we can postulate that ashes from some of these identified eruptions might be found in the neighboring Pliocene-Pleistocene sedimentary basins, and further to the south and east/southeast likely as cryptotephras.

6. Conclusion

Six new explosive eruption events were recognized in the eruption history of KV, a volcanic system located in the central parts of Southeastern Europe (N. Macedonia). Single-crystal sanidine $^{40}Ar/^{39}Ar$ dating revealed an older period at 4.0–3.5 Ma, which includes the units of GR04 (3.93 ± 0.04 Ma), PO02p (3.83 ± 0.03 Ma), VI02 (3.73 ± 0.04 Ma) and PO03 (3.61 ± 0.02 Ma), and a younger period at 3.0–2.5 Ma including the units of GR08d (2.66 ± 0.03 Ma) and GR11 (2.56 ± 0.02 Ma), together with the previously recognized eruptions of Šumovit Greben at 2.9–2.8 Ma. These ages contributed to redefine the eruptive activity of the volcanic system, as the 4.0–2.5 Ma period was considered mainly quiescent. In addition to their importance in understanding the KV volcanic activity, the identified tephra layers help to constrain the evolution of the Mariovo basin, as these occur intermittently with the lacustrine-fluvial sediments.

The pyroclastic layers (mainly massive tuff-lapilli tuff and massive lithic breccia) are deposited from phreatomagmatic (VI02) and subplinian eruptions (GR08), pyroclastic flows (GR04, PO02p), and block-and-ash flows (GR11, PO03) in the volcano-sedimentary Mariovo basin, west of the volcanic system. Eruption products from the older period (4.0–3.5 Ma) imply sequential evacuation of closely emplaced, discrete, melt-dominant bodies, as inferred from the differences in their glass geochemical data. The younger period might represent the evacuation of a compositionally zoned single-melt body. The continuous pyroclastic sequence of the latter records an explosive-to-effusive transition over a short period (2.66–2.56 Ma), starting with massive lapilli tuff and tuff layers deposited from subplinian or phreatomagmatic explosive eruption, which progressed into a dome-collapse-related block-and-ash flow deposit. This transition in the eruptive style is also supported by a gradual decrease in water content accompanied by an increase in crystallinity in the erupted products.

The ages and glass compositions of the newly recognized pyroclastic layers show no overlap with those of previously studied tephra layers from the Kožuf-Voras volcanic system or other volcanic sources (e.g., Aegean arc). Therefore, these could serve as new marker layers even for the wider region.

CRediT authorship contribution statement

Kata Molnár: Conceptualization, Investigation, Resources, Visualization, Writing – original draft, Writing – review & editing. **Pierre Lahitte:** Formal analysis, Methodology, Resources, Writing – original draft, Writing – review & editing. **Zsolt Benkó:** Funding acquisition, Resources, Writing – review & editing. **János Szepesi:** Investigation, Writing – original draft, Writing – review & editing. **Maxim Portnyagin:** Formal analysis, Methodology, Resources, Writing – original draft, Writing – review & editing. **Daniel Frick:** Methodology, Resources, Writing – review & editing. **Samuele Agostini:** Formal analysis, Methodology, Resources, Writing – original draft, Writing – review & editing. **Sebastien Nomade:** Methodology, Resources, Writing – review & editing, Formal analysis. **Maria Giuditta Fellin:** Formal analysis, Methodology, Resources, Writing – original draft, Writing – review & editing. **Colin Maden:** Methodology, Resources, Writing – review & editing. **Ivan Boev:** Resources, Writing – review & editing. **Blažo Boev:** Resources, Writing – review & editing. **Marjan Temovski:** Investigation, Resources, Visualization, Writing – original draft, Writing – review & editing.

Declaration of competing interest

The authors declare that they have no known competing financial interests or personal relationships that could have appeared to influence the work reported in this paper.

Acknowledgments

This research was supported by the European Union and the State of Hungary, financed by the European Regional and Development Fund in the project of GINOP-2.3.2-15-2016-00009 'ICER' project, co-financed by the French-Hungarian Cooperation Program TÉT-2018-00018 and

TelluS-SYSTER 2021 program of INSU, CNRS. The article is part of the NKFI-OTKA PD 135396 project. KM was supported by the 'Fellowship for researchers with young children' of the Hungarian Academy of Sciences. We thank Mario Thöner (GEOMAR) for his assistance with electron probe analysis and Ulrike Westernströer (CAU Kiel) for her assistance with LA-ICP-MS analysis. This work is also supported by the MTA–HUN-REN CSFK Lendület "Momentum" PannonianVolcano Research Group (LP2024-9). Fieldwork was carried out under Research permit No. 14-47/2, issued by the Geological Survey of the Republic of North Macedonia. (U—Th)/He analyses were carried out in the framework of Europlanet 2024 RI. Glass geochemical data for comparison were downloaded from the GEOROC database (https://georoc.eu/) on 4 September 2024 using the following parameters: geological setting = convergent margins: Aegean Arc; type of material = volcanic glass. SA acknowledges EPOS JRU Italia for support in Sr—Nd isotope data collection and in lab maintenance.

Appendix A. Supplementary data

Supplementary data to this article can be found online at https://doi.org/10.1016/j.jvolgeores.2026.108564.

Data availability

The data used in this work has been shared in the Supplementary Materials.

References

Agostini, S., Doglioni, C., Innocenti, F., Manetti, P., Tonarini, S., Savaşçin, M.Y., 2007. The transition from subduction-related to intraplate Neogene magmatism in the Western Anatolia and Aegean area. In: Beccaluva, L., Bianchini, G., Wilson, M. (Eds.), Cenozoic Volcanism in the Mediterranean Area. Geological Society of America. https://doi.org/10.1130/2007.2418(01).

Agostini, S., Di Giuseppe, P., Manetti, P., Savaşçın, M.Y., Conticelli, S., 2022. Geochemical and isotopic (Sr-Nd-Pb) signature of crustal contamination in Na-alkali basaltic magmas of South-East Turkey. Ital. J. Geosci. 141 (3), 363–384. https://doi.org/10.3301/IJG.2022.21.

Arsovski, M., 1997. Tectonic of Macedonia. Rudarsko-Geol. Fac. Štip, p. 306 (in Macedonian).

Benet, D., Costa, F., Pedreros, G., Cardona, C., 2021. The volcanic ash record of shallow magma intrusion and dome emplacement at Nevados de Chillán Volcanic complex, Chile. J. Volcanol. Geotherm. Res. 417, 107308. https://doi.org/10.1016/J.JVOLGEORES.2021.107308.

Boehnke, P., Harrison, T.M., 2014. A meta-analysis of geochronologically relevant half-lives: what's the best decay constant? Int. Geol. Rev. 56, 905–914. https://doi.org/10.1080/00206814.2014.908420.

Boev, B., Ilijovski, Z., 2013. Mineralogical- geochemical characteristic of the Neogene sediments at the coal mine of Zivojno in the Pelagonia depression. Geol. Maced. 27, 55–63.

Boev, I., Ivanova, T.Š., 2024. Age of the volcanoclastic sedimentary rocks of the Vitačevo volcanic plateau (Kožuf Mountain), North Macedonia. Geol. Maced. 38, 5–14.

Boev, B., Yanev, Y., 2001. Tertiary magmatism within the Republic of Macedonia: a review. Acta Vulcanol. 13, 57–71.

Branney, M.J., Kokelaar, P., 2002. Pyroclastic Density Currents and the Sedimentation of Ignimbrites. Geological Society of London. https://doi.org/10.1144/GSL.MEM.2003.027.

Brlek, M., Trinajstić, N., Gaynor, S.P., Kutterolf, S., Hauff, F., Schindlbeck-Belo, J., Šuica, S., Wang, K.L., Lee, H.Y., Watts, E., Georgiev, S.V., Brčić, V., Špelić, M., Mišur, I., Kukoč, D., Schoene, B., Lukács, R., 2024. Spread and frequency of explosive silicic volcanism of the Carpathian-Pannonian Region during early Miocene: clues from the SW Pannonian Basin and the Dinarides. J. Volcanol. Geotherm. Res. 455, 108215. https://doi.org/10.1016/J.JVOLGEORES.2024.108215.

Brown, R.J., Andrews, G.D.M., 2015. Deposits of pyroclastic density currents. In: The Encyclopedia of Volcanoes, pp. 631–648. https://doi.org/10.1016/B978-0-12-385938-9.00036-5.

Brown, R.J., Branney, M.J., Maher, C., Dávila-Harris, P., 2010. Origin of accretionary lapilli within ground-hugging density currents: evidence from pyroclastic couplets on Tenerife. GSA Bull. 122, 305–320. https://doi.org/10.1130/B26449.1.

Burchfiel, B.C., Nakov, R., Dumurdzanov, N., Papanikolaou, D., Tzankov, T., Serafimovski, T., King, R.W., Kotzev, V., Todosov, A., Nurce, B., 2008. Evolution and dynamics of the Cenozoic tectonics of the South Balkan extensional system. Geosphere 4, 919–938. https://doi.org/10.1130/GES00169.1.

Cashman, K.V., Sparks, R.S.J., Blundy, J.D., 2017. Vertically extensive and unstable magmatic systems: a unified view of igneous processes. Science (1979) 355, eaag3055. https://doi.org/10.1126/science.aag3055.

Chamberlain, K.J., Wilson, C.J.N., Wallace, P.J., Millet, M.-A., 2015. Micro-analytical perspectives on the Bishop Tuff and its Magma Chamber. J. Petrol. 56, 605–640. https://doi.org/10.1093/petrology/egv012.

Clift, P., Blusztajn, J., 1999. The trace-element characteristics of Aegean and Aeolian volcanic arc marine tephra. J. Volcanol. Geotherm. Res. 92, 321–347. https://doi.org/10.1016/S0377-0273(99)00059-1.

Cooper, G.F., Wilson, C.J.N., Millet, M.-A., Baker, J.A., 2016. Generation and rejuvenation of a supervolcanic magmatic system: a case study from Mangakino Volcanic Centre, New Zealand. J. Petrol. 57, 1135–1170. https://doi.org/10.1093/petrology/egw035.

Cvetković, V., Prelević, D., Downes, H., Jovanović, M., Vaselli, O., Pécskay, Z., 2004. Origin and geodynamic significance of Tertiary postcollisional basaltic magmatism in Serbia (Central Balkan Peninsula). Lithos 73, 161–186. https://doi.org/10.1016/j.lithos.2003.12.004.

Dumurdzanov, N., Krstic, N., Mihajlovic, D., Ognjanova-Rumenova, N., Petrov, G., 2003. New data on stratigraphy of the Neogene and Pleistocene in Mariovo, Macedonia. Geol. Maced. 17, 43–52.

Dumurdzanov, N., Serafimovski, T., Burchfiel, B.C., 2005. Cenozoic tectonics of Macedonia and its relation to the South Balkan extensional regime. Geosphere 1, 1–22. https://doi.org/10.1130/GES00006.1.

Eleftheriadis, G., Castorina, F., Soldatos, T., Masi, U., 2003. Geochemical and Sr–Nd isotopic evidence for the genesis of the Late Cainozoic Almopia volcanic rocks, 78. Central Macedonia, Greece). Mineralogy and Petrology, pp. 21–36. https://doi.org/10.1007/s00710-002-0217-0.

Harangi, S., Downes, H., Seghedi, I., 2006. Tertiary-Quaternary subduction processes and related magmatism in the Alpine-Mediterranean region. Geol. Soc. Lond. Mem. 32, 167–190. https://doi.org/10.1144/GSL.MEM.2006.032.01.10.

Harmon, L.J., Gualda, G.A.R., Gravley, D.M., Smithies, S.L., Deering, C.D., 2024. The Whakamaru magmatic system (Taupō Volcanic Zone, New Zealand), part 1: evidence from tephra deposits for the eruption of multiple magma types through time. J. Volcanol. Geotherm. Res. 445, 107966. https://doi.org/10.1016/j.jvolgeores.2023.107966.

Hildreth, W., Wilson, C.J.N., 2007. Compositional zoning of the Bishop Tuff. J. Petrol. 48, 951–999. https://doi.org/10.1093/petrology/egm007.

Hoult, H., Kennedy, B.M., Nichols, A.R.L., Cronin, S., Watson, L., 2024. Conduit armouring preceding explosive activity at an andesitic stratovolcano, an example from Taranaki Mounga, New Zealand. J. Volcanol. Geotherm. Res. 455, 108214. https://doi.org/10.1016/J.JVOLGEORES.2024.108214.

Hutchison, W., Gabriel, I., Plunkett, G., Burke, A., Sugden, P., Innes, H., Davies, S., Moreland, W.M., Krüger, K., Wilson, R., Vinther, B.M., Dahl-Jensen, D., Freitag, J., Oppenheimer, C., Chellman, N.J., Sigl, M., McConnell, J.R., 2024. High-resolution ice-core analyses identify the Eldgjá eruption and a cluster of Icelandic and trans-continental Tephras between 936 and 943 CE. J. Geophys. Res. Atmos. 129, e2023JD040142. https://doi.org/10.1029/2023JD040142.

Janka, P., Sági, T., Temovski, M., Benkó, Z., Lahitte, P., Molnár, K., 2024. A Kožuf-Voras vulkáni rendszer lávadómjainak kőzettani vizsgálata. In: Buday, T., Csámer, Á., McIntosh, R.W., Molnár, K., Virág, A. (Eds.), Ahány Kő, Annyi Történet.14. Kőzettani És Geokémiai Vándorgyűlés Előadás- És Poszterkivonatok. HUN-REN Atommagkutató Intézet, Debrecen, Magyarország, p. 138 (in Hungarian).

Janković, S., Boev, B., Serafimovski, T., 1997. Magmatism and tertiary mineralization of the Kozuf metallogenetic district, the Republic of Macedonia with particular reference to the Alsar deposit, Magmatizam i tercierna mineralizacija vo Kozhufskata oblast vo Makedonija so poseben osvrt na naogjalishteto Alshar. Faculty of Mining and Geology Geological Department, Macedonia, The Former Yugoslav Republic of.

Keller, J., Ryan, W.B.F., Ninkovich, D., Altherr, R., 1978. Explosive volcanic activity in the Mediterranean over the past 200,000 yr as recorded in deep-sea sediments. GSA Bull. 89, 591–604. https://doi.org/10.1130/0016-7606(1978)89<591:EVAITM>2.0.CO;2.

Kolios, N., Innocenti, F., Manetti, P., Peccerillo, A., Giuliani, O., 1980. The pliocene volcanism of the Voras Mts (Central Macedonia, Greece). Bull. Volcanol. 43, 553–568. https://doi.org/10.1007/BF02597692.

Lane, C.S., Lowe, D.J., Blockley, S.P.E., Suzuki, T., Smith, V.C., 2017. Advancing tephrochronology as a global dating tool: applications in volcanology, archaeology, and palaeoclimatic research. Quat. Geochronol. 40, 1–7. https://doi.org/10.1016/J.QUAGEO.2017.04.003.

Lee, J.-Y., Marti, K., Severinghaus, J.P., Kawamura, K., Yoo, H.-S., Lee, J.B., Kim, J.S., 2006. A redetermination of the isotopic abundances of atmospheric Ar. Geochim. Cosmochim. Acta 70, 4507–4512. https://doi.org/10.1016/j.gca.2006.06.1563.

Lehmann, St, Barcikowski, J., von Quadt, A., Gallhofer, D., Peytcheva, I., Heinrich, C.A., Serafimovski, T., 2013. Geochronology, geochemistry and isotope tracing of the Oligocene magmatism of the Buchim–Damjan–Borov Dol ore district: implications for timing, duration and source of the magmatism. Lithos 180–181, 216–233. https://doi.org/10.1016/j.lithos.2013.09.002.

Lowe, D.J., 2011. Tephrochronology and its application: a review. Quat. Geochronol. 6, 107–153. https://doi.org/10.1016/J.QUAGEO.2010.08.003.

Ludwig, K.R., 2012. User's Manual for Isoplot Version 3.75–4.15: A Geochronological Toolkit for Microsoft Excel. Berkeley Geochronological Center Special Publication, p. 5.

Lustrino, M., Wilson, M., 2007. The circum-Mediterranean anorogenic Cenozoic igneous province. Earth Sci. Rev. 81, 1–65. https://doi.org/10.1016/J.EARSCIREV.2006.09.002.

MacDonald, A., Ubide, T., Mollo, S., Taddeucci, J., 2024. Spatial and temporal mush heterogeneity during eruptions recorded in clinopyroxene from the 2021 paroxysms at Mt. Etna, Italy. Contrib. Mineral. Petrol. 179, 99. https://doi.org/10.1007/s00410-024-02174-5.

Manville, V., 2001. Sedimentology and history of Lake Reporoa: an Ephemeral Supra-Ignimbrite Lake, Taupo Volcanic Zone, New Zealand. In: Volcaniclastic Sedimentation in Lacustrine Settings, pp. 109–140. https://doi.org/10.1002/9781444304251.ch6.

Molnár, K., Lahitte, P., Dibacto, S., Benkó, Z., Agostini, S., Dönczö, B., Ionescu, A., Milevski, I., Szikszai, Z., Kertész, Z., Temovski, M., 2022. The westernmost Late Miocene–Pliocene volcanic activity in the Vardar zone (North Macedonia). Int. J. Earth Sci. 111, 749–766. https://doi.org/10.1007/s00531-021-02153-2.

Molnár, K., Lahitte, P., Dönczö, B., Arató, R., Szepesi, J., Benkó, Z., Nomade, S., Gätjen, J., Dibacto, S., Temovski, M., 2023. Unravelling the pre-eruptive conditions of the rhyolitic Šumovit Greben lava dome from clinopyroxene-dominant glomeroporphyritic clots. Contrib. Mineral. Petrol. 178, 83. https://doi.org/10.1007/s00410-023-02066-0.

Mueller, S., Scheu, B., Kueppers, U., Spieler, O., Richard, D., Dingwell, D.B., 2011. The porosity of pyroclasts as an indicator of volcanic explosivity. J. Volcanol. Geotherm. Res. 203, 168–174. https://doi.org/10.1016/J.JVOLGEORES.2011.04.006.

Niespolo, E.M., Rutte, D., Deino, A.L., Renne, P.R., 2017. Intercalibration and age of the Alder Creek sanidine 40Ar/39Ar standard. Quat. Geochronol. 39, 205–213. https://doi.org/10.1016/j.quageo.2016.09.004.

Peccerillo, A., 2005. Plio-Quaternary Volcanism in Italy. Springer Berlin, Heidelberg, p. 365.

Peccerillo, A., Taylor, S.R., 1976. Geochemistry of eocene calc-alkaline volcanic rocks from the Kastamonu area, Northern Turkey. Contrib. Mineral. Petrol. 58, 63–81. https://doi.org/10.1007/BF00384745.

Pe-Piper, G., Piper, D.J.W., 2007. Neogene backarc volcanism of the Aegean: new insights into the relationship between magmatism and tectonics. In: Beccaluva, L., Bianchini, G., Wilson, M. (Eds.), Cenozoic Volcanism in the Mediterranean Area. Geological Society of America. https://doi.org/10.1130/2007.2418(02).

Perkins, M.E., Nash, B.P., 2002. Explosive silicic volcanism of the Yellowstone hotspot: the ash fall tuff record. GSA Bull. 114, 367–381. https://doi.org/10.1130/0016-7606(2002)114<0367:ESVOTY>2.0.CO;2.

Platz, T., Cronin, S.J., Cashman, K.V., Stewart, R.B., Smith, I.E.M., 2007. Transition from effusive to explosive phases in andesite eruptions — a case-study from the AD1655 eruption of Mt. Taranaki, New Zealand. J. Volcanol. Geotherm. Res. 161, 15–34. https://doi.org/10.1016/J.JVOLGEORES.2006.11.005.

Ponomareva, V., Portnyagin, M., Pendea, I.F., Zelenin, E., Bourgeois, J., Pinegina, T., Kozhurin, A., 2017. A full holocene tephrochronology for the Kamchatsky Peninsula region: applications from Kamchatka to North America. Quat. Sci. Rev. 168, 101–122. https://doi.org/10.1016/J.QUASCIREV.2017.04.031.

Popa, R.-G., Bachmann, O., Huber, C., 2021. Explosive or effusive style of volcanic eruption determined by magma storage conditions. Nat. Geosci. 14, 781–786. https://doi.org/10.1038/s41561-021-00827-9.

Portnyagin, M.V., Ponomareva, V.V., Zelenin, E.A., Bazanova, L.I., Pevzner, M.M., Plechova, A.A., Rogozin, A.N., Garbe-Schönberg, D., 2020. TephraKam: geochemical database of glass compositions in tephra and welded tuffs from the Kamchatka volcanic arc (northwestern Pacific). Earth Syst. Sci. Data 12, 469–486. https://doi.org/10.5194/essd-12-469-2020.

Renne, P.R, Balco, G., Ludwig, K.R., Mundil, R., Min, K., 2011. Response to the comment by W.H. Schwarz et al. on "Joint determination of 40K decay constants and 40Ar*/40K for the Fish Canyon sanidine standard, and improved accuracy for $_{40}Ar/_{39}Ar$ geochronology" by P.R. Renne et al. (2010). Geochim Cosmochim Acta 75, 5097–5100. https://doi.org/10.1016/j.gca.2011.06.021.

Schmid, S.M., Fügenschuh, B., Kounov, A., Maţenco, L., Nievergelt, P., Oberhänsli, R., Pleuger, J., Schefer, S., Schuster, R., Tomljenović, B., Ustaszewski, K., van Hinsbergen, D.J.J., 2020. Tectonic units of the Alpine collision zone between Eastern Alps and western Turkey. Gondwana Res. 78, 308–374. https://doi.org/10.1016/j.gr.2019.07.005.

Schwarzkopf, L.M., Schmincke, H.U., Cronin, S.J., 2005. A conceptual model for block-and-ash flow basal avalanche transport and deposition, based on deposit architecture of 1998 and 1994 Merapi flows. J. Volcanol. Geotherm. Res. 139, 117–134. https://doi.org/10.1016/J.JVOLGEORES.2004.06.012.

Steenbrink, J., Van Vugt, N., Hilgen, F.J., Wijbrans, J.R., Meulenkamp, J.E., 1999. Sedimentary cycles and volcanic ash beds in the lower Pliocene lacustrine succession of Ptolemais (NW Greece): discrepancy between 40Ar/39Ar and astronomical ages. Palaeogeogr. Palaeoclimatol. Palaeoecol. 152, 283–303. https://doi.org/10.1016/S0031-0182(99)00044-9.

Steenbrink, J., Hilgen, F.J., Krijgsman, W., Wijbrans, J.R., Meulenkamp, J.E., 2006. Late Miocene to Early Pliocene depositional history of the intramontane Florina–Ptolemais–Servia Basin, NW Greece: interplay between orbital forcing and tectonics. Palaeogeogr. Palaeoclimatol. Palaeoecol. 238, 151–178. https://doi.org/10.1016/J.PALAEO.2006.03.023.

Sulpizio, R., Capra, L., Sarocchi, D., Saucedo, R., Gavilanes-Ruiz, J.C., Varley, N.R., 2010. Predicting the block-and-ash flow inundation areas at Volcán de Colima (Colima, Mexico) based on the present day (February 2010) status. J. Volcanol. Geotherm. Res. 193, 49–66. https://doi.org/10.1016/J.JVOLGEORES.2010.03.007.

Sun, S.-S., McDonough, W.F., 1989. Chemical and isotopic systematics of oceanic basalts: implications for mantle composition and processes. Geol. Soc. Lond. Spec. Publ. 42, 313–345. https://doi.org/10.1144/GSL.SP.1989.042.01.19.

Temovski, M., Wieser, A., Marchhart, O., Braun, M., Madarász, B., Kiss, G.I., Palcsu, L., Ruszkiczay-Rüdiger, Z., 2024. Pleistocene valley incision, landscape evolution and inferred tectonic uplift in the central parts of the Balkan Peninsula – insights from the geochronology of cave deposits in the lower part of Crna Reka basin (N. Macedonia). Geomorphology 445, 108994. https://doi.org/10.1016/j.geomorph.2023.108994.

Tomlinson, E.L., Smith, V.C., Albert, P.G., Aydar, E., Civetta, L., Cioni, R., Çubukçu, E., Gertisser, R., Isaia, R., Menzies, M.A., Orsi, G., Rosi, M., Zanchetta, G., 2015. The major and trace element glass compositions of the productive Mediterranean volcanic sources: tools for correlating distal tephra layers in and around Europe. Quat. Sci. Rev. 118, 48–66. https://doi.org/10.1016/J.QUASCIREV.2014.10.028.

Trafton, K.R., Giachetti, T., 2021. The morphology and texture of Plinian pyroclasts reflect their lateral sourcing in the conduit. Earth Planet. Sci. Lett. 562, 116844. https://doi.org/10.1016/J.EPSL.2021.116844.

Vougioukalakis, G., 1994. The Pliocene volcanites of the Voras mountain, Central Macedonia, Greece. Bull. Geol. Soc. Greece XXX, 223–240.

Vougioukalakis, G., 2002. Petrological, Geochemical and Volcanological Study of the Almopias Pliocene Volcanic Formations and their Correlation with the Geothermal Manifestations in the Area. PhD Thesis. Aristotle University of Thessaloniki, p. 303 (in Greek).

Vougioukalakis, G.E., Satow, C.G., Druitt, T.H., 2019. Volcanism of the South Aegean volcanic arc. Elements 15, 159–164. https://doi.org/10.2138/gselements.15.3.159.

Wagner, B., Vogel, H., Francke, A., Friedrich, T., Donders, T., Lacey, J.H., Leng, M.J., Regattieri, E., Sadori, L., Wilke, T., Zanchetta, G., Albrecht, C., Bertini, A., Combourieu-Nebout, N., Cvetkoska, A., Giaccio, B., Grazhdani, A., Hauffe, T., Holtvoeth, J., Joannin, S., Jovanovska, E., Just, J., Kouli, K., Kousis, I., Koutsodendris, A., Krastel, S., Lagos, M., Leicher, N., Levkov, Z., Lindhorst, K., Masi, A., Melles, M., Mercuri, A.M., Nomade, S., Nowaczyk, N., Panagiotopoulos, K., Peyron, O., Reed, J.M., Sagnotti, L., Sinopoli, G., Stelbrink, B., Sulpizio, R., Timmermann, A., Tofilovska, S., Torri, P., Wagner-Cremer, F., Wonik, T., Zhang, X., 2019. Mediterranean winter rainfall in phase with African monsoons during the past 1.36 million years. Nature 573, 256–260. https://doi.org/10.1038/s41586-019-1529-0.

Walker, G.P.L., 1973. Mount Etna and the 1971 eruption - Lengths of lava flows. Philos. Trans. R. Soc. A Math. Phys. Eng. Sci. 274, 107–118.

Wilson, C.J.N., Cooper, G.F., Chamberlain, K.J., Barker, S.J., Myers, M.L., Illsley-Kemp, F., Farrell, J., 2021. No single model for supersized eruptions and their magma bodies. Nat. Rev. Earth Environ. 2, 610–627. https://doi.org/10.1038/s43017-021-00191-7.

Yanev, Y., Boev, B., Doglioni, C., Innocenti, F., Manetti, P., Pecskay, Z., Tonarini, S., D'Orazio, M., 2008. Late Miocene to Pleistocene potassic volcanism in the Republic of Macedonia. Mineral. Petrol. 94, 45–60. https://doi.org/10.1007/s00710-008-0009-2.

Zindler, A., Hart, S.R., 1986. Chemical geodynamics. Annu. Rev. Earth Planet. Sci. 14, 493–570. https://doi.org/10.1146/annurev.ea.14.050186.002425.